Top-of-Atmosphere Radiance-to-Flux Conversion in the SW Domain for the ScaRaB-3 Instrument on Megha-Tropiques

MICHEL VIOLLIER*

Laboratoire de Météorologie Dynamique/IPSL/CNRS, Ecole Polytechnique, Palaiseau, France

CARSTEN STANDFUSS

Noveltis, Ramonville-St. Agne, France

OLIVIER CHOMETTE

Laboratoire de Météorologie Dynamique/IPSL/CNRS, Ecole Polytechnique, Palaiseau, France

ARNAUD QUESNEY

Noveltis, Ramonville-St. Agne, France

(Manuscript received 8 December 2008, in final form 15 May 2009)

ABSTRACT

The earth radiation budget (ERB) is the difference between the solar absorbed flux and the terrestrial emitted flux. These fluxes are calculated from satellite measurements of outgoing shortwave (SW) and longwave (LW) radiances using empirical or theoretical models of the radiation anisotropy, which are called angular distribution models (ADMs). Owing to multidirectional measurement analyses and synergy with multispectral information at subpixel scale, the ADM developed for the NASA Clouds and the Earth's Radiant Energy System (CERES) mission is presently the best knowledge and has to be taken into account for future ERB missions, such as the Indian–French Megha-Tropiques mission to be launched in 2010. This mission will carry an ERB instrument called the Scanner for Radiation Budget (ScaRaB). To prepare the algorithms for the ScaRaB ADM retrievals, the artificial neural network (ANN) method described by the CERES team has been adopted and improved by replacing the broadband (BB) radiances by narrowband (NB) radiances from the auxiliary channels of ScaRaB as input variables of the ANN. This article is restricted to the SW domain, the most critical case, and shows that the flux error is reduced by 60% compared to the former ERB Experiment–like model. The rms differences with the CERES fluxes are around 8.4 W m^{-2}. ScaRaB/Megha-Tropiques measurements have a 4 times lower spatial resolution than those of the CERES/Tropical Rainfall Measuring Mission (TRMM). The impact of this spatial degradation has also been explored. There is a small systematic bias of about 1.5 W m^{-2} (or an absolute albedo error of 0.0015) and the rms differences are less than 3 W m^{-2}; this is not significant compared to the overall error budget. For the radiance-to-flux conversion in the SW domain, the BB and NB ANN methods will be implemented in the ScaRaB/Megha-Tropiques data processing in order to provide SW flux estimates with an accuracy that is as consistent as possible with CERES results.

1. Introduction

During the last decades, two National Aeronautics and Space Administration (NASA) missions [Earth Radiation Budget Experiment (ERBE; Barkstrom et al. 1989) and Clouds and the Earth's Radiant Energy System (CERES; Wielicki et al. 1996)] have been devoted to the estimation of the earth radiation budget (ERB). Additional contributions have also been provided by the Scanner for Radiation Budget (ScaRaB; Kandel et al. 1998; Duvel et al. 2001) and Geostationary Earth Radiation Budget (GERB) instruments (Harries et al. 2005; Dewitte et al. 2008). All these ERB missions are based on broadband (BB) radiometers, which measure the shortwave (SW) reflected solar radiation (0.2–4 μm) and the

* Deceased.

Corresponding author address: Olivier Chomette, Laboratoire de Météorologie Dynamique/IPSL/CNRS, Ecole Polytechnique, 91190 Palaiseau, France.
E-mail: chomette@lmd.polytechnique.fr

DOI: 10.1175/2009JTECHA1264.1

longwave (LW) emitted terrestrial radiation (4–100 μm) with high absolute accuracy (1%–2%), owing to onboard calibration modules (blackbody, lamps, and solar diffuser) and careful cross-checking analyses. In 2010, the French–Indian mission Megha-Tropiques (MT) will carry a third model of the ScaRaB instrument and two microwave passive radiometers [Microwave Analysis and Detection of Rain and Atmospheric Structures (MADRAS) and Sounder for Atmospheric Profiling of Humidity in the Intertropics by Radiometry (SAPHIR)] for precipitation and water vapor. The goal of Megha-Tropiques is to observe and analyze the energy and water exchanges in the tropical atmosphere. The orbit is inclined by 20° to the equator. This inclination allows improving the time sampling in the observed tropical zone (30°S–30°N). At the altitude of 867 km, the instantaneous ScaRaB field of view (FOV) of 48 milliradians corresponds to a geographical footprint of approximately 40 km squared at nadir.

Excluding multidirectional observation missions such as Polarization and Directionality of the Earth's Reflectances (POLDER; Deschamps et al. 1994), the conversion between radiance and hemispherical flux at the top of the atmosphere (TOA) is classically obtained by application of scene type and observation geometry–dependent anisotropy models [often referred to as angular distribution models (ADMs), which are further defined in section 2a]. The ERBE ADMs (Suttles et al. 1988, 1989) and corresponding inversion methods (Wielicki and Green 1989) were based on a crude distinction of only 12 scene types (composed of 5 surface types and 4 cloud cover intervals). A better distinction for the ERBE instruments was not achievable; the information on scene content from the available two broadband channels is limited. The CERES approach to improve anisotropy correction (Loeb et al. 2003a,b, 2005, 2007) is based on synergy with collocated measurements at subpixel sampling from a multispectral visible–infrared (VIS–IR) imager. In this configuration, the function of the imager is to provide the scene identification (including relevant information on cloud fraction, cloud phase, cloud optical thickness, and cloud emissivity). This allows the consideration of about 600 scene types within the operational CERES processing. The corresponding ADMs are considered as best knowledge models to describe anisotropy and will be used as reference (i.e., considered ''truth'') in this study.

The Megha-Tropiques objectives require accurate instantaneous flux estimates, which cannot be obtained with the ERBE-like processing. On the other hand, the ScaRaB data processing cannot directly use the CERES ADM algorithms, because on board Megha-Tropiques there is no imager similar to the Visible Infrared Scanner (VIRS) or Moderate Resolution Imaging Spectroradiometer (MODIS) that is able to provide precise scene identification and to select the appropriate ADM. However, with the CERES ADM being the best knowledge, the post-CERES experiments must provide flux estimates as close as possible to CERES. This paper explains how we plan to fulfill this goal. It is restricted to the SW domain because the solar reflected flux concentrates the major part of the angular errors. Starting with the flux estimates of CERES/Tropical Rainfall Measuring Mission (TRMM) at 10-km resolution, we adopt the artificial neural network (ANN) approach described by Loukachine and Loeb (2003, 2004). Second, we show how the substitution of the broadband radiances by narrowband (NB) radiances as input variables of the ANN improves this method. Indeed, ScaRaB carries narrowband channels in the visible and infrared domains in addition to the broadband channels. These channels are expected to enable a better geophysical characterization of the scene content associated to flux measurements in broadband channels. Because the anisotropy of the radiance field is strongly dependent on the scene content, it can be concluded that auxiliary (narrowband) measurements are better predictors for the radiance anisotropy as well. Finally, because the ADM a priori depends on the instantaneous field of view of the instruments, we will study the impact of the spatial resolution on these results.

2. Data and methods

a. ADM definition

The ERB instruments measure broadband radiances in the SW and LW domains. From satellite, these radiances $L(\theta_0, \theta, \varphi)$ relate to the viewing direction, which is defined in the SW domain by three angles: local viewing zenith angle (VZA) θ, local solar zenith angle (SZA) θ_0, and relative azimuth (RAZ) φ between the local observation and solar planes with zenith. For a given SZA θ_0 the reflective flux $F(\theta_0)$ at the top of the atmosphere is the integral of radiation in the upper hemisphere,

$$F(\theta_0) = \int_0^{\pi/2} \int_0^{2\pi} L(\theta_0, \theta, \phi) \cos\theta \sin\theta \, d\theta \, d\phi. \quad (1)$$

From the statistical analysis of multiangle observations and computations of Eq. (1), ADM tables or anisotropy function R have been computed to convert radiance to flux for ERBE (Suttles et al. 1988, 1989) and CERES (Loeb et al. 2003a,b, 2005, 2007). By definition, these tables depend not only on the angles but also on the characteristics of the observed terrestrial scene. Indeed, the anisotropy is more pronounced for clear ocean than for thick clouds. The radiance-to-flux conversion is then defined by the equation

$$F(\theta) = \frac{\pi L(\theta_0, \theta, \phi)}{R_I(\theta_0, \theta, \phi)}, \quad (2)$$

where R_I is the anisotropy function, or ADM, for the scene identified by index I.

b. CERES TRMM dataset

TRMM has a 350-km circular precessing orbit with a 35° inclination angle. For this altitude, the spatial resolution of CERES on TRMM is 10 km at nadir. As a training dataset for ScaRaB/Megha-Tropiques, we have selected the CERES/TRMM dataset. Indeed, because CERES/TRMM observations are limited to 38°S–38°N, the CERES/TRMM ADM is more representative for the tropics than CERES on *Terra* or *Aqua*, which are in polar sun-synchronous orbits. Furthermore, TRMM has a 46-day nodal precession cycle, so all SZAs over a region are sampled for this period, which is close to the corresponding 51 days for Megha-Tropiques. The precision of the ANN anisotropy correction depends on the representation of the observation/geophysical conditions the model is finally applied to. Compared to a polar orbit mission, a tropical mission such as MT, with limited seasonal variation, will then find a suitable learning dataset easily, especially because of the existence of CERES/TRMM. There are 8 months of CERES/TRMM data from January to August 1998. CERES operated in three scan modes: across track, along track, and rotating azimuth plane (RAP). From the 77 days operated in RAP and along-track modes, radiances have been measured from a multitude of viewing configurations. Together with scene identification inferred from multispectral information at subpixel scale provided by VIRS, Loeb et al. (2003a) have developed a specific ADM for this mission.

For the ADM selection, the scene identification is based on retrievals of cloud and atmospheric properties applied to the collocated VIRS radiances at subpixel scale, then averaged over a CERES footprint. Clear-sky scenes are defined as CERES footprints with less than 0.1% cloud fraction; the number of cloud fraction intervals other than clear sky is 12, 5, and 2 over ocean, land, and snow/ice-covered pixels, respectively. Relative wind speed intervals and aerosol contents are distinguished in cases of clear ocean. However, no specific aerosol ADMs are derived, but a continuous correction is applied, based on lookup tables (LUTs) derived from Discrete Ordinate Radiative Transfer (DISORT) model simulations over a wide range of aerosol optical thickness. Land and desert surfaces are further divided into low-to-moderate tree/shrub coverage (LMTS), moderate-to-high tree/shrub coverage (MHTS), dark desert (DD), and bright desert (BD). Cloud phase is distinguished. Finally, cloudy scenes are separated into 14 and 6 relative cloud optical depth intervals over ocean and land, respectively. This leads to 586 SW ADM scene types [index I in Eq. (2)]. All the essential parameters (radiances, fluxes, and scene identification) are available in the Single Scanner Footprint (SSF) CERES products.

The validation of this new ADM has been intensively studied in the second CERES/TRMM paper by Loeb et al. (2003b). The first test is that the long-term flux averages must not have a dependence on the viewing geometry or at least a smaller dependence than former ADMs. It was shown that the relative variations in the TOA albedo, as a function of the observation angles, were less than 2%. Another validation method is the comparison of two methods for computing monthly means. Indeed, over a sufficiently long period, all the viewing geometries are sampled and radiances can be sorted and averaged into discrete angular bins. Then, a direct integration can be calculated from Eq. (1). Comparing this direct integration to the regional mean flux allows isolating the ADM error contributions from the other error sources. It was shown that the differences were very small: 0.5 W m^{-2} for both SW and LW. A third validation method deals with the instantaneous flux. The along-track mode provides means to compare estimates from nadir and oblique viewing directions. For all sky and averaged over a 1° latitude by 1° longitude grid, the rms differences of flux estimates at nadir and at 65° are 7.5% (SW) and 2.3% (LW), about a factor of 2 less than for the former ERBE ADM. However, these figures provide consistency checks but no absolute accuracy, because the true value of the flux cannot be measured. To go further and to give an indirect estimate of flux error, Loeb et al. (2003b) have simulated radiances from theoretical models and applied different ADMs. Then, they compare the nadir–oblique consistency check to the flux error. They found rms errors of 10.8 and 3.5 W m^{-2} (SW and LW, respectively).

In conclusion, CERES ADMs for TOA fluxes must be considered as reference because of the excellent quality of input data (i.e., multidirectional broadband measurements in synergy with multispectral information at subpixel scale) and because of widespread validation studies. The CERES/TRMM flux estimates will be considered truth in this study.

c. Neural network methods of radiance-to-flux conversion

1) WITH BROADBAND CHANNELS (BB ANN)

A possible failure of the imager during CERES operations renders the operational CERES anisotropy correction inapplicable. Therefore, the CERES team at

NASA has developed a backup solution for anisotropy correction, based on an artificial neural network (ANN) approach of the type feed-forward error backpropagation (FFEB; Loukachine and Loeb 2003, 2004). The network corresponds to a perceptron multilayer and consists of an input layer (observables), two hidden layers, and an output layer (ADM). This method is independent of explicit scene identification (though networks are generated separately for a small number of surface types, all are applicable to all-sky conditions). In the SW domain, the input variables are the SZA, VZA, and RAZ observation angles and the SW and LW radiances. As learning datasets, Loukachine and Loeb (2003) use the 68 days of CERES RAP data. To get a reduced and consistent observation set, the data are stratified by the input variables according to a limited number of intervals. Mean value of the input variables and of the ADM are calculated for each data bin when the number of observations is sufficient. Because input variables are also ScaRaB observables, this approach is perfectly applicable to ScaRaB.

We have regenerated this approach under similar learning conditions in order to validate the ScaRaB algorithms with the results of Loukachine and Loeb (2003) and to control the method for further improvements. For the generation of the SW ADMs, we have trained the FFEB multilayer ANN in the same structure proposed by Loukachine and Loeb (2004). The two hidden layers, L1 and L2, contain 7 and 11 neurons, respectively, with a tangent sigmoid activation function (linear activation function for the output layer). The input layer and first hidden layer are partially connected in order to separate weakly and strongly correlated input parameters. Corresponding to the stratification variables of the training dataset, the input vectors for the flux retrievals have been defined by VZA, SZA, RAZ, LW BB radiance (L_{LW}), and SW BB radiance (L_{SW}). The networks have been trained (i.e., optimization of the weights affected to each connection) by using the Stuttgart Neural Network Simulator (SNNS) software, version 4.2 (available online at http://www-ra.informatik.uni-tuebingen.de/SNNS/). Six neural networks have been optimized corresponding to the six surface types distinguished by the SW ADM type applied in the operational CERES processing (ocean/glint, ocean/no glint, land LMTS, land MHTS, bright desert, and dark desert). Each neural network has been trained using the generalized delta rule with a varying learning rate and a constant momentum (backpropagation momentum function for SNNS with a learning rate p1 = 0.1, a learning momentum p2 = 0.6, a flat spot elimination value p3 = 0, and a maximum difference back propagated p4 = 1.0×10^{-8}). The network training performance is characterized by the sum of the quadratic differences between the whole ADMs contained in the training dataset and the ADMs retrieved in the output of the network from the input given by the training dataset [sum of square errors (SSE)]. For each network, hundreds of random initializations of the network weights and bias (from 0 to 1) have been tested. The one that conducts to the lowest SSE is finally retained. For each initialization, the training proceeds up to 100 000 iterations over the entire training set. For each training iteration, the decision about the next iteration is based on the SSE gradient from the current SSE and the last one. If the SSE decreases, then the new weight, bias, and SSE values are kept for the next iteration. The learning rate is increased by 0.001 until it reaches the maximum allowed value (0.5). If the SSE increases, then the ANN proceeds to the next iteration by keeping SSE, weight, and bias values from the preceding iteration. The learning rate is decreased by 0.0009 or 0.0002, depending on whether the SSE has increased or decreased at the preceding iteration, respectively. The training process stops if the learning rate is ≤ 0 or if the number of iterations is higher than 100 000. For all trainings we have done, the process was stopped by the learning rate constraint. Loukachine and Loeb (2003) have applied a brusque decrease of the learning rate to 0.05 in the case of a SSE increase. Comparing the two methods of learning rate adjustment in the case of increasing SSE, we state that the described method of smoother decrease leads to higher performances (smallest SSE), particularly because of a higher number of iterations taken into account during the training process.

2) With narrowband channels (NB ANN)

We plan further improvement by using the two ScaRaB auxiliary narrowband channels: visible (0.5–0.7 μm) and infrared window (10.5–12.5 μm). These channels are expected to enable a better geophysical characterization of the scene content associated to flux measurements in broadband channels. Several studies were developed for this research with encouraging results (Stubenrauch et al. 1993; Li and Trishchenko 1999; Chang et al. 2000). Because the anisotropy of the radiance field is strongly dependent on the scene content, it is expected that auxiliary (narrowband) measurements are better predictors for the radiance anisotropy. In this context, we have modified the initial learning datasets, including narrowband radiances, constructed from VIRS narrowband radiances. To simulate the VIS ScaRaB channel (0.50–0.70 μm), we use the channel 1 of VIRS (0.535–0.711 μm) centered at 0.623 μm. Our hypothesis is that the ScaRaB-VIS and VIRS-1 reflectances are identical. The window IR ScaRaB channel is defined between 10.5 and 12.5 μm, which is different from the IR

CERES channel (from 8 to 12 μm). To simulate the IR ScaRaB channel, we use channels 4 and 5 of VIRS, which are centered at 10.826 and 12.028 μm, respectively, with a bandwidth of about 1.05 μm. Here, the hypothesis is that the ScaRaB IR brightness temperature is equal to the average brightness temperature in VIRS channels 4 and 5.

In spite of the expected physical gain in the content of the learning data, some shortcomings with respect to the initial learning data described in section 2b(1) are inevitable. One of the disadvantages of the modified learning datasets is their restricted coverage in terms of observation geometry. The simulation of ScaRaB measurements by association of VIRS and CERES measurements requires a common viewing geometry for both instruments. This excludes the use of CERES SSF data in RAP scan mode; to construct a dataset of consistent CERES broadband and VIRS narrowband radiances, only CERES data in across-track scan mode (limited to VZA $< 50°$) are useful. The SW learning dataset is structured as before, except that the SW and LW radiances are replaced by the VIS and IR radiances, respectively, as stratification variables. The interval limits for stratification are adjusted to the corresponding variation range of the new variables.

d. Spatial degradation

The methods described previously are derived from CERES/TRMM measurements and therefore correspond to a resolution of 10 km at nadir. ScaRaB/Megha-Tropiques measurements have a 4 times lower spatial resolution. Decrease of the spatial resolution with VZA is in first approximation (neglecting orbit height differences) proportional between CERES/TRMM and ScaRaB/MT. Therefore, it is convenient to consider a certain number of adjacent CERES/TRMM pixels as representative for one ScaRaB/MT pixel, independently of VZA.

The applicability of ADMs derived at a spatial scale of 10 km at nadir to measurements at a 4 times lower resolution must then be investigated. Under the hypothesis that low-resolution (here, ScaRaB/MT) fluxes and radiances F_S and L_S are linearly composed of N high-resolution (here, CERES) subpixel fluxes and radiances F_i and L_i and with R_i as the applicable anisotropy factor to each subpixel, the flux F_S estimated at low resolution is given by

$$F_S = \frac{\pi}{N}\sum_{i=1}^{N}\frac{L_i}{R_i}. \tag{3}$$

If measurements are obtained at the lower resolution, the estimated flux F'_S is obtained under the assumption of a homogeneous flux distribution; that is, L_i/R_i is constant within the pixel, and thus

$$F'_S = \pi\frac{\sum_{i=1}^{N} L_i}{\sum_{i=1}^{N} R_i}. \tag{4}$$

The error introduced by the degradation in spatial resolution is simply the difference $(F'_S - F_S)$.

It disappears if, within a pixel S,

- the variation of the observation geometry is negligible (i.e., if R_i is constant within S for any homogeneous scene) and
- the scene is actually homogeneous (otherwise R_i varies because of scene heterogeneity).

Consequently, errors increase with increasing dimension of S, implying stronger variations in observation geometry and a higher probability of scene heterogeneity. We will investigate the contribution of the relatively low spatial resolution of ScaRaB/MT to the total error flux estimation error. The objective is to verify that the error resulting from a degraded spatial resolution is small against the intrinsic error of the applied ADMs assessed by ANN methods. In this case, we can consider that ADMs generated from measurements at CERES/TRMM spatial resolution are applicable at ScaRaB/MT resolution also.

The impact of reduced spatial resolution on flux retrievals is first analyzed on original CERES fluxes and ADMs. These being considered as reference values, the corresponding results represent the accuracy loss of flux estimates at 40-km spatial resolution with respect to high-resolution measurements averaged over the same spatial resolution. This investigation addresses a physical phenomenon and does not depend at all on the choice of the ADM to be implemented in the ScaRaB level 2 processing. For verification purpose, we have analyzed the impact on the ANN-based ADM, where application of Eq. (4) is not required because we can estimate R directly from the spatially degraded input radiances and adjusted viewing geometry. In case of an acceptable impact of spatial resolution on the flux retrieval, it is expected that this impact is approximately the same if using an ADM with a certain precision. Otherwise, ADM errors would be significantly correlated with the impact of spatial degradation.

3. Results

a. The learning datasets

For the broadband case, the input variables are the same as in Loukachine and Loeb (2003); that is, VZA (in

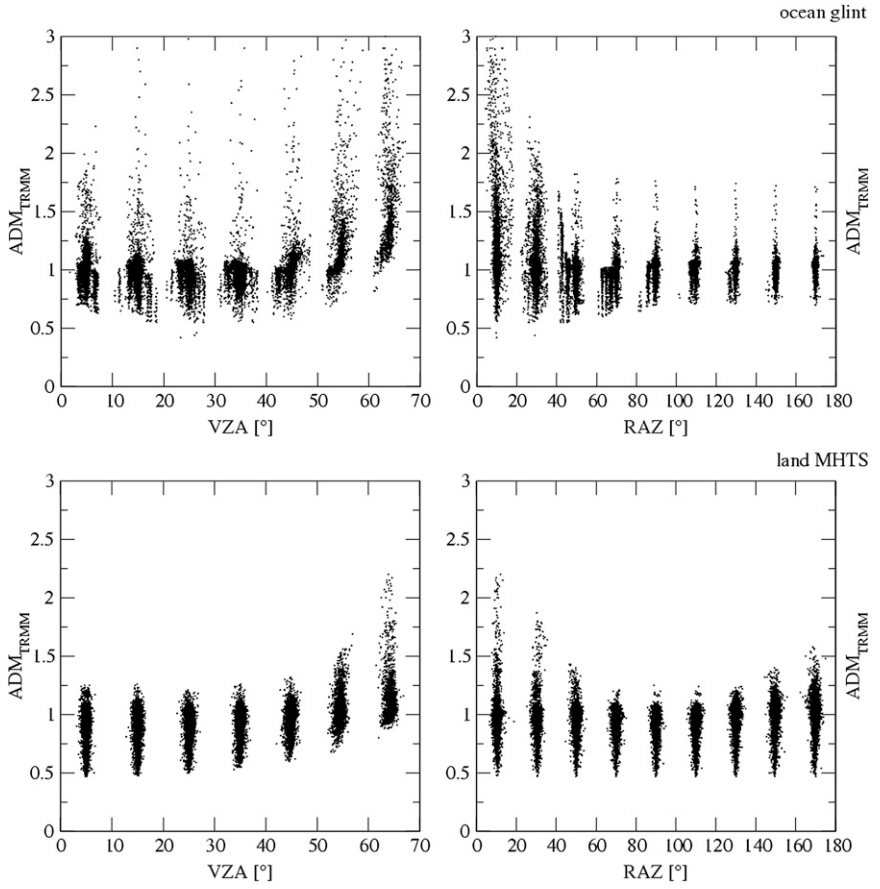

FIG. 1. Scatterplots of the ADM vs (left) the VZA and (right) RAZ in the 5-variable stratified BB data. Each data point corresponds to a stratification bin: (top) high ADM variability for ocean/glint and (bottom) low ADM variability for land MHTS.

degrees), RAZ (in degrees), L_{LW} (in W m^{-2} sr^{-1}), the SZA (in degrees), and L_{SW} (in W m^{-2} sr^{-1}). All inputs are normalized to the maximum value for each variable: 90° for VZA and SZA, 180° for RAZ, 150 W m^{-2} sr^{-1} for L_{LW}, and 300 W m^{-2} sr^{-1} for L_{SW}. For the narrowband case, the SW and LW radiances are replaced by the VIS and IR radiances, respectively. They are normalized to 110 and 15 W m^{-2} sr^{-1}, respectively. The learning dataset has been developed from stratification into intervals (bins) of these input vectors. Several learning datasets are defined according to the surface type (ocean/glint, ocean/no glint, land with sparse and dense vegetation, and bright and dark deserts). The filling rate of theoretically possible bins (255 150) is quite low: about 7%. This is due to either physical constraints (e.g., the hottest scenes cannot be the brightest) or correlations of binned variables (e.g., the brightest scenes are associated with small SZA). For the surface types ocean/glint and land, Fig. 1 presents examples of relations within the SW learning dataset, the ADM versus VZA and RAZ, which shows an exceptional ADM variability for the surface type ocean/glint.

To assess the intrinsic accuracy that can be expected by using the current stratification of the learning dataset, it is interesting to investigate the variability of the anisotropy factor per stratification bin for the six surface types. As an example, Fig. 2 (top) presents the standard deviation of anisotropy factors over individual measurements within each bin of the broadband learning dataset for the surface types ocean/glint and ocean/no glint. This variability is shown as a function of VZA. Generally, the highest variability is associated to high SZA (except for ocean/no glint), high VZA, and—most strikingly—to low RAZ. In terms of surface types, we state the exceptionally high variability for ocean/glint. The lowest variability is obtained for ocean/no glint. For all land surface types (not shown), the variability is only slightly above the variability shown for ocean/no glint. The average standard deviation of individual anisotropy factors within a stratification interval of the learning datasets is 0.18 for ocean/glint and 0.03–0.04 for all other scenes. For a global average flux Fsw = (1368 × 0.5 × 0.3) = 205 W m^{-2} (over the daylight hemisphere), we

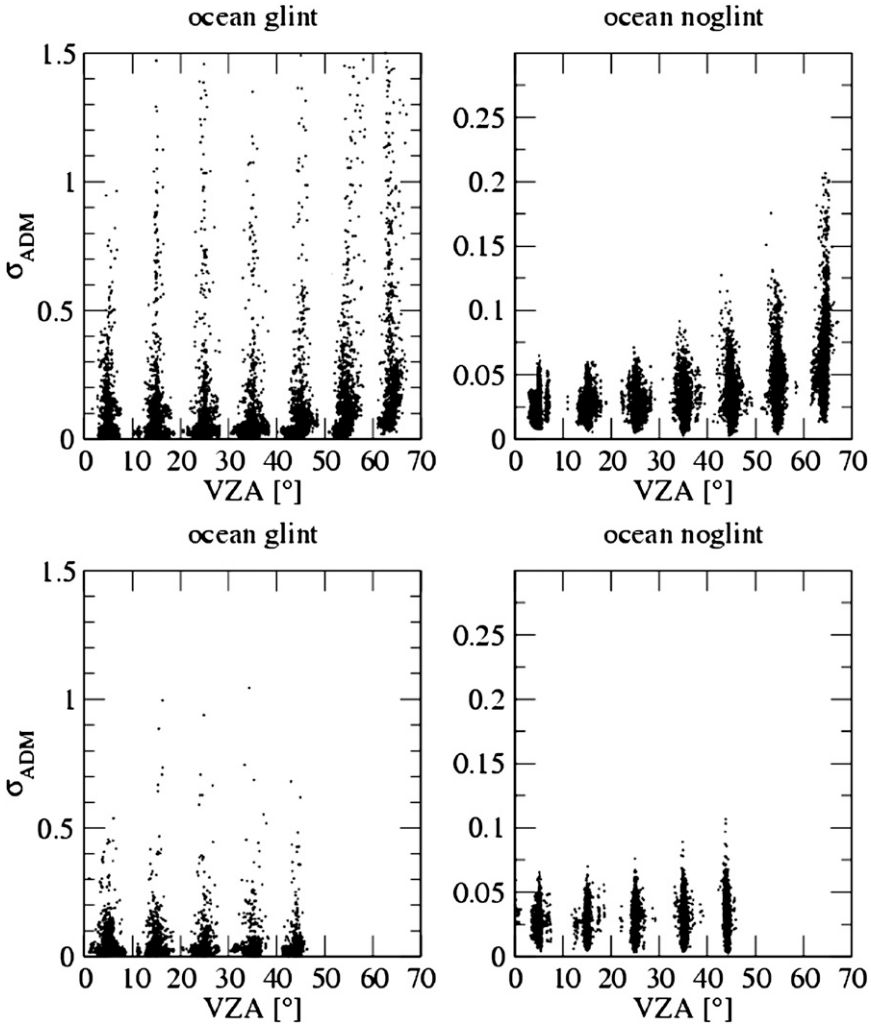

FIG. 2. Standard deviation of the SW anisotropy factor within stratification bins of the SW learning dataset as a function of VZA bins for the cases of (left) ocean/glint and (right) ocean/no glint from (top) the BB learning dataset (mean and standard deviations of 0.18 and 0.04, respectively) and (bottom) the NB learning dataset (mean and standard deviations of 0.04 and 0.02, respectively).

obtain an intrinsic precision of about 6–8 W m^{-2} (except for ocean/glint conditions) for the learning dataset. Thus, we must accept a performance decrease of any anisotropy model derived from the current SW learning dataset for ocean/glint compared to the performances of all other surface types.

For the narrowband training dataset, comparison with the broadband case is shown on Fig. 2 (bottom). The average standard deviation of individual anisotropy factors within a stratification interval of the learning datasets decreases strongly from 0.18 to 0.04 for ocean/glint and by about 30% to 0.02–0.03 for all other scenes. These numbers must be interpreted with caution because of the different angular coverage of the two learning datasets. If we compare at equivalent VZA bins, we can see that a significant gain is obtained mainly for ocean/glint conditions, which justifies the use of narrowband channels. The stratification with NB radiances then improves the association between bin content and ADM classification. This is a condition sine qua non to work with the ScaRaB auxiliary channels; otherwise, we could conclude that narrowband radiances do not better predict the anisotropy than broadband radiances.

The learning results of the six trained networks are gathered in Table 1 for the broadband and narrowband networks. The comparison of results with those obtained by Loukachine and Loeb (2003) suggests that our trained neural networks are of similar performance, even of better performance, except for the ocean/glint surface type. For this type, the complexity of the relation

TABLE 1. ANN learning performance for BB and NB methods. The results found by Loukachine and Loeb (2003) for the BB method are shown in parentheses. The relative error is the relative differences between the retrieved ADM (ADM_{ANN}) and the target value from the training set (ADM_{TS}), or $(ADM_{ANN} - ADM_{TS})/ADM_{TS}$ in percent.

	BB network				NB network			
Surface types	No. of relations (NbRel) contained in the training set	No. of processed iterations	Relative error (%)		NbRel contained in the training set	No. of processed iterations	Relative error (%)	
			Mean	Std dev			Mean	Std dev
BD	20 632	24 647	−0.00 (0.08)	2.14 (3.14)	4893	36 331	−0.04	1.51
DD	24 438	9285	0.09 (0.16)	3.87 (4.22)	7051	13 223	0.02	1.94
Land LMTS	29 500	11 776	−0.08 (0.14)	3.24 (3.88)	8379	17 336	−0.09	2.31
Land MHTS	27 772	13 945	0.07 (0.14)	2.91 (4.05)	7318	15 715	0.16	2.63
Ocean/glint	20 513	6294	1.50 (0.34)	10.29 (6.40)	6891	13 032	0.10	3.61
Ocean/no glint	20 813	11 336	0.52 (0.34)	4.31 (5.84)	5873	31 165	0.07	2.07

between the input and the ADM could not be well represented. The learning results of the narrowband trained networks are shown on the right side of Table 1. Compared to the broadband networks, the ADM errors are significantly smaller.

b. Performance analysis

The ANN performance is analyzed with independent instantaneous data. According to Loukachine and Loeb (2003), the ANN-based flux retrievals are more accurate than the former ERBE retrievals, both in terms of VZA independence and in differences by comparison with the truth (the CERES SSF fluxes). The SW mean differences are negligible (-0.3 W m^{-2}) compared to ERBE differences (3.6 W m^{-2}). The standard deviations in the differences between the ANN and SSF SW flux estimates are 14.2 W m^{-2} compared to 17.1 W m^{-2}. The corresponding rms differences are 14.2 W m^{-2} compared to 17.5 W m^{-2}. Such improvement is also found from our own computations. Table 2 summarizes the compared average performances of the ERBE-like and ANN broadband approaches over 32 days of across-track mode (two periods of 16 days between 15 February and 3 April and between 15 July and 29 August 1998). For the broadband approach, the ANN ADM overall performance is convincing and suggests an error reduction on the order of 50%–60% with respect to the ScaRaB ERBE-like processing, except for ocean/glint scenes.

For comparison with the broadband approach, Table 2 gives also the results for the ANN method using narrowband channels. In terms of rms differences, SW NB ANN performs better than SW BB ANN by 40%. The most spectacular improvements are noticed for ocean scenes, both glint and no glint, whereas improvements for land scenes are smaller. These results would confirm that the input variables (narrowband instead of broadband radiances) are better predictors for anisotropy. Narrowband radiances provide higher contrast than broadband radiances between ocean and clouds.

c. Impact of the spatial resolution

According to the method presented in section 2d, this section presents the impact of the degraded spatial resolution from 10 to 40 km. The objective is not to quantify the effect of spatial degradation over the entire validation dataset but to quantify its magnitude relative to the intrinsic ADM errors. The spatial degradation effect is mainly due to scene heterogeneity, which is modulated by viewing geometry. Because typical scene heterogeneity can be represented by a global dataset over one day, we define two days within the validation dataset as the investigation period to cover different observation geometries relative to the sun corresponding to different local time of the ascending node (LTAN) of the orbit: 23 August 1998 (LTAN 3 h and 30 min) and 29 August 1998 (LTAN 0 h and 22 min).

Note that, for 23 August, no small solar zenith angles were present. Global results of the difference $F'_S - F_S$ defined by Eqs. (3) and (4) are presented in Table 3. For the purpose of verification, the second line (ANN) shows

TABLE 2. The 32-day average of SW flux errors (bias ± standard deviation) in W m^{-2} of the ERBE-like, BB-ANN, and NB-ANN flux retrievals. The 32 days cover two periods of 16 days between 15 Feb and 3 Apr and between 15 Jul and 29 Aug 1998.

Scene type	All	All but ocean/glint	Ocean/glint	Ocean/no glint	Land and desert (max from the 4 classes)
ERBE like	−12.70 ± 18.27	−13.14 ± 17.46	−11.22 ± 20.52	−17.44 ± 16.57	−07.41 ± 17.40
BB ANN	−03.87 ± 14.33	−02.48 ± 09.21	−09.77 ± 23.68	−03.59 ± 08.76	−01.00 ± 10.00
NB ANN	−00.70 ± 08.44	−00.54 ± 07.14	−01.46 ± 13.36	−00.83 ± 06.29	−00.81 ± 9.50

TABLE 3. Impact of degraded spatial resolution from CERES/TRMM to ScaRaB/Megha-Tropiques (global bias ± standard deviation over 1-day datasets for 23 and 29 Aug 1998). Based on Eqs. (3) and (4), the flux differences, ADM ratios, and albedo α differences are reported. The impact is computed separately for original CERES and for ANN ADM-based flux estimations. Differences in the LW domain, almost zero, are shown for comparison.

		SW			LW	
1998		$F' - F$ (W m^{-2})	R'/R	$\alpha' - \alpha$	$F' - F$ (W m^{-2})	R'/R
23 Aug	CERES	+1.20 ± 2.80	+0.9940 ± 0.0141	+0.0016 ± 0.0036	−0.010 ± 0.085	+1.0000 ± 0.0004
	ANN	+1.17 ± 2.52	+0.9938 ± 0.0126	+0.0016 ± 0.0033	+0.002 ± 0.061	+1.0000 ± 0.0003
29 Aug	CERES	+1.15 ± 2.42	+0.9941 ± 0.0141	+0.0015 ± 0.0031	−0.010 ± 0.080	+1.0000 ± 0.0004
	ANN	+1.14 ± 2.26	+0.9940 ± 0.0118	+0.0015 ± 0.0029	+0.000 ± 0.055	+1.0000 ± 0.0003

the impact on the ANN-based ADM. In that case, the application of Eq. (4) is not required, because we can estimate R directly from the spatially degraded input radiances and adjusted viewing geometry. The impact is the same for the two models. For comparison, the impact of spatial degradation in the LW domain is also shown and demonstrated as negligible against the typical precision of current LW ADMs of about 2.5–3 W m^{-2}. In the SW domain, spatial degradation to the scale of ScaRaB/Megha-Tropiques leads to an additional uncertainty of 2.5–3 W m^{-2} (rms) of the flux retrieval as compared to 14 W m^{-2} for the precision of the BB ANN ADM. Estimations for the ANN ADM are slightly below those obtained for the CERES ADM, which suggests that the spatial heterogeneity of anisotropy predicted by ANN is slightly underestimated. Nevertheless, the difference is not significant in the overall error budget.

At first glance, surprisingly, the impact of spatial degradation is stronger for 23 August, when no small solar zenith angles are present, whereas the intrinsic ADM accuracy is lower for 29 August. A striking feature is a stable bias of about +1.2 W m^{-2} (corresponding to an absolute albedo error of 0.15%) associated with spatial degradation. Figures 3 and 4 present the mean albedo error as a function of VZA, SZA, and RAZ for 23 and 29 August 1998, respectively. No particular features are observed in terms of VZA dependence; the bias of about 0.15% is constant with VZA and stable in time. In terms of SZA dependence, it becomes obvious that the positive bias is systematically increasing with SZA up to 70°. In particular, errors associated to overhead sun are below the average, which explains why the overall error is lower for 29 August than for 23 August. In conclusion, the SW ADMs derived from measurements of CERES/TRMM are applicable to ScaRaB/Megha-Tropiques without harm.

4. Conclusions

The present study has implemented anisotropy correction schemes based on the artificial neural network

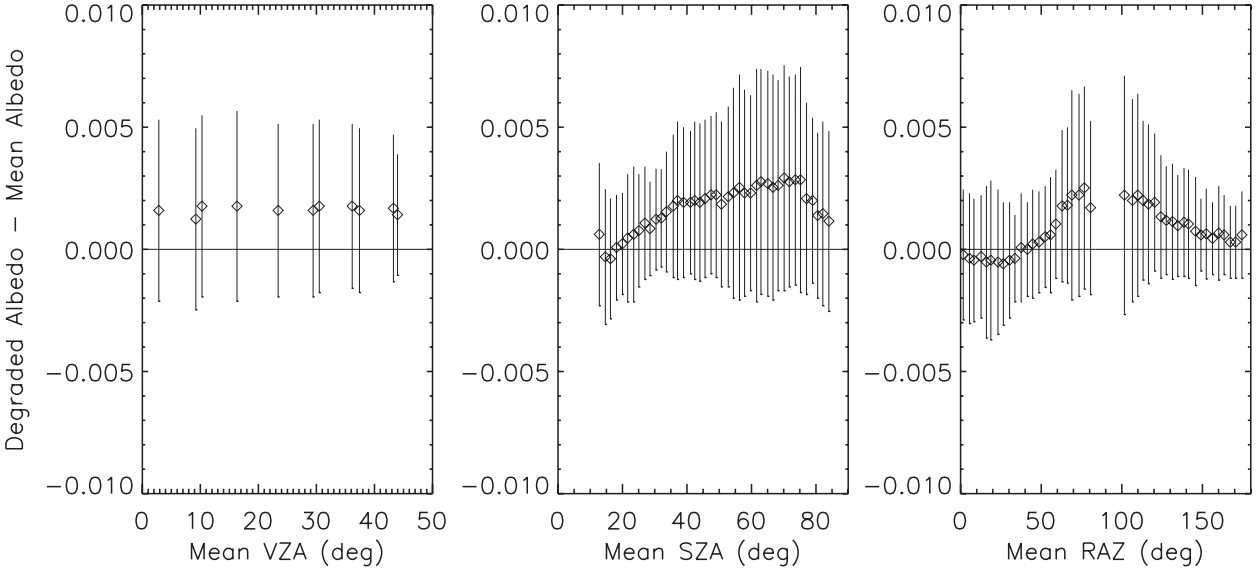

FIG. 3. Impact of the spatial resolution. CERES albedo difference (mean ±1 standard deviation) α'SW − αSW as a function of (left) VZA, (middle) SZA, and (right) RAZ for 23 Aug 1998.

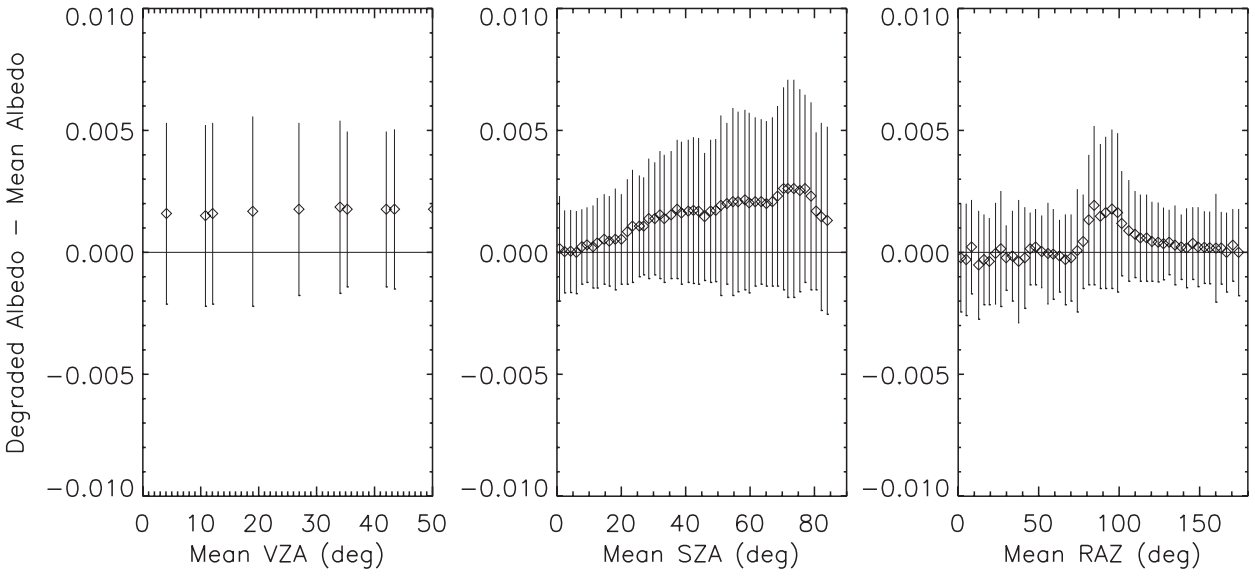

FIG. 4. As in Fig. 3, but for 29 Aug 1998.

(ANN) and has assessed their performance in view of defining the operational level 2 processing for the ScaRaB mission on Megha-Tropiques. The ANN approach is inspired from work performed by the NASA CERES team (Loukachine and Loeb 2003) in view of generating a fairly accurate backup anisotropy correction algorithm in case of a failure of the accompanying imager. We demonstrate that the CERES backup method for SW anisotropy correction is a promising approach for improving the operational ScaRaB/MT anisotropy correction. Moreover, this method can be largely improved by replacing the broadband radiances by narrowband radiances that are available from the auxiliary ScaRaB channels. The assessment of the new anisotropy correction schemes indicates a considerable progress in view of an improved ScaRaB instantaneous flux retrieval and hints at a potential breakthrough for the SW component. Quantitative conclusions of this paper are threefold.

- Based on broadband radiances as input variables, the SW ANN anisotropy model reduces the error of instantaneous SW fluxes with respect to the ERBE-like processing by 34%, to about 14 W m^{-2}. Anisotropy correction in ocean/glint conditions is critical, however. The ANN model shows, systematically, a poor performance in specific observation geometries. Over ocean/glint conditions, the approach provides, globally, no improvement with respect to the current ScaRaB processing. For all other scenes, the error is reduced to 45%, or about 10 W m^{-2}. In principle, this ANN anisotropy model is applicable as such to ScaRaB/Megha-Tropiques; all input variables are direct ScaRaB observables.
- Developed for VZA angles $<50°$, an improved SW ANN anisotropy model has been assessed, where narrowband radiances replace broadband radiances as input variables. The narrowband ANN anisotropy model reduces the error of instantaneous SW fluxes with respect to the ERBE-like processing by 60%, to about 9 W m^{-2}. The SW flux error is reduced to 2–3 times the LW flux error; this may be considered particularly interesting for the consolidated understanding of the energy budget of tropical convective systems, which is one of the Megha-Tropiques mission objectives. With respect to the initial SW ANN model, spectacular improvements are stated over ocean: in particular, in ocean/glint conditions.
- ADMs derived on CERES/TRMM measurements at relatively high spatial resolution (10 km at nadir) are applicable to ScaRaB/Megha-Tropiques (40 km at nadir) without significant impact on the overall error budget (stable bias +1.2 W m^{-2}; rmse <3 W m^{-2}).

Acknowledgments. The authors thank Konstantin Loukachine and Norman Loeb for their helpful responses to our various solicitations on their ADM and ANN works. We also thank our colleagues Michel Capderou, Rémy Roca, and Filipe Aires for helpful discussion. The CERES SSF data were obtained from the NASA Langley Research Center Atmospheric Sciences Data Center. The neural networks have been trained using the Stuttgart Neural Network Simulator (SNNS) software (available online at http://www-ra.informatik.uni-tuebingen.de/SNNS/). The study has been supported by CNES for the preparation of the Megha-Tropiques data processing.

REFERENCES

Barkstrom, B. R., and Coauthors, 1989: Earth Radiation Budget Experiment (ERBE) archival and April 1985 results. *Bull. Amer. Meteor. Soc.,* **70,** 1254–1262.

Chang, F.-L., Z. Li, and A. P. Trishchenko, 2000: The dependence of TOA reflectance anisotropy on cloud properties inferred from ScaRaB satellite data. *J. Appl. Meteor.,* **39,** 2480–2493.

Deschamps, P. Y., F. M. Breon, M. Leroy, A. Podaire, A. Bricaud, J. C. Buriez, and G. Seze, 1994: The POLDER mission: Instrument characteristics and scientific objectives. *IEEE Trans. Geosci. Remote Sens.,* **32,** 598–615.

Dewitte, S., L. Gonzalez, N. Clerbaux, A. Ipe, C. Bertrand, and B. De Paepe, 2008: The Geostationary Earth Radiation Budget Edition 1 data processing algorithms. *Adv. Space Res.,* **41,** 1906–1913.

Duvel, J. P., and Coauthors, 2001: The ScaRaB–Resurs earth radiation budget dataset and first results. *Bull. Amer. Meteor. Soc.,* **82,** 1397–1408.

Harries, J. E., and Coauthors, 2005: The Geostationary Earth Radiation Budget Project. *Bull. Amer. Meteor. Soc.,* **86,** 945–960.

Kandel, R., and Coauthors, 1998: The ScaRaB earth radiation budget dataset. *Bull. Amer. Meteor. Soc.,* **79,** 765–783.

Li, Z., and A. Trishchenko, 1999: A study toward an improved understanding of the relationship between visible and shortwave measurements. *J. Atmos. Oceanic Technol.,* **16,** 347–360.

Loeb, N. G., N. M. Smith, S. Kato, W. F. Miller, S. K. Gupta, P. Minnis, and B. A. Wielicki, 2003a: Angular distribution models for top-of-atmosphere radiative flux estimation for the Clouds and the Earth's Radiant Energy System instrument on the Tropical Rainfall Measuring Mission satellite. Part I: Methodology. *J. Appl. Meteor.,* **42,** 240–265.

——, K. Loukachine, N. Manalo-Smith, B. A. Wielicki, and D. F. Young, 2003b: Angular distribution models for top-of-atmosphere radiative flux estimation from the Clouds and the Earth's Radiant Energy System instrument on the Tropical Rainfall Measuring Mission satellite. Part II: Validation. *J. Appl. Meteor.,* **42,** 1748–1769.

——, S. Kato, K. Loukachine, and N. Manalo-Smith, 2005: Angular distribution models for top-of-atmosphere radiative flux estimation from the Clouds and the Earth's Radiant Energy System instrument on the *Terra* satellite. Part I: Methodology. *J. Atmos. Oceanic Technol.,* **22,** 338–351.

——, ——, ——, ——, and D. R. Doelling, 2007: Angular distribution models for top-of-atmosphere radiative flux estimation from the Clouds and the Earth's Radiant Energy System instrument on the *Terra* satellite. Part II: Validation. *J. Atmos. Oceanic Technol.,* **24,** 564–584.

Loukachine, K., and N. G. Loeb, 2003: Application of an artificial neural network simulation for top-of-atmosphere radiative flux estimation from CERES. *J. Atmos. Oceanic Technol.,* **20,** 1749–1757.

——, and ——, 2004: Top-of-atmosphere flux retrievals from CERES using artificial neural network. *Remote Sens. Environ.,* **93,** 381–390.

Stubenrauch, C. J., J.-P. Duvel, and R. S. Kandel, 1993: Determination of longwave anisotropic emission factors from combined broad- and narrowband radiance measurements. *J. Appl. Meteor.,* **32,** 848–856.

Suttles, J. T., and Coauthors, 1988: Angular radiation models for Earth-atmosphere system. Volume 1: Shortwave radiation. NASA Rep. RP 1184, 144 pp.

——, R. N. Green, G. L. Smith, B. A. Wielicki, I. J. Walker, V. R. Taylor, and L. L. Stowe, 1989: Angular radiation models for Earth-atmosphere system. Volume 2: Longwave radiation. NASA Rep. RP 1184-VOL-2, 88 pp.

Wielicki, B. A., and R. N. Green, 1989: Cloud identification for ERBE radiative flux retrieval. *J. Appl. Meteor.,* **28,** 1133–1146.

——, B. R. Barkstrom, E. F. Harrison, R. B. Lee, G. L. Smith, and J. E. Cooper, 1996: Clouds and the Earth's Radiant Energy System (CERES): An Earth Observing System experiment. *Bull. Amer. Meteor. Soc.,* **77,** 853–868.